Ceramics International (xxxx) xxxx–xxxx

Contents lists available at ScienceDirect

Ceramics International

journal homepage: www.elsevier.com/locate/ceramint

Radioluminescence, thermoluminescence and dosimetric properties of ZnO ceramics

Larisa Grigorjeva[a,*], Aleksejs Zolotarjovs[a], Sergej Yu Sokovnin[b,c], Donats Millers[a], Krisjanis Smits[a], Vladislav G. Il`ves[b,c]

[a] Institute of Solid State Physics, University of Latvia, Kengaraga 8, LV-1063, Riga, Latvia
[b] Institute of Electrophysics, Ural Branch, Russian Academy of Sciences, 106 Amundsen Street, Yekaterinburg 620016, Russia
[c] Ural Federal University, 19 Mira Street, Yekaterinburg 620016, Russia

ARTICLE INFO

Keywords:
A. ZnO ceramic
B. Sintering
C. Thermostimulated luminescence
D. Dosimetry

ABSTRACT

Two types of ZnO ceramics were fabricated and characterized by XRD, SEM methods. The radioluminescence spectra were measured within the 300–550 K range. The defect luminescence band peaking at ~2.35 eV is the dominant one in radioluminescence spectra in both of the fabricated ceramics. The thermostimulated luminescence (TSL) glow-curves were measured after X-ray irradiation at 300 K. It was concluded that the complex overlapping peak within the 320–450 K temperature range consists of two components (~360–375 K and 400–420 K). The ratio of component intensities differs in both ceramics. The positions of high temperature TSL components (480–520 K) also differ in both samples; therefore not only sintering conditions but also the properties of the initial powder are very important for characteristics of TSL. A linear dependence of peak intensity on irradiation dose was observed up to ~3 kGy for ceramic 1 and up to 9 kGy for ceramic 2.

1. Introduction

In recent years the ZnO attracted many researchers due to its possible applications as transparent conductive electrodes [1], particle detectors [2], fast scintillators [3], sensors [4] and others.

Due to recent advances in nanotechnology it is possible to obtain ZnO in nanocrystal form as well as ZnO coatings or thin films resulting in the large amount of new studies and new applications for this material. The most comprehensive review article [5] summarizes information of mechanical, chemical, electrical, and optical properties of ZnO.

The luminescence of two types is usually observed – the near-band or exciton luminescence and defects luminescence. The exciton luminescence is in near-UV range (375 nm) and is very fast: for example, in ZnO single crystal free exciton luminescence lifetime at room temperature is 440 ps and can be used for fast scintillators [3,5]. The defect luminescence is in visible range: 480–650 nm and exhibits non-exponential decay up to hundreds of microseconds [6]. The detailed mechanism of 2.3 eV luminescence is not still proven despite numerous studies. The peak position of defect luminescence band, its intensity and decay kinetics are very sensitive to the type and morphology of ZnO as well as to the synthesis method used, annealing conditions, doping and other parameters. Unfortunately, up to now the defect pairs responsible for the luminescence are not completely identified. The intrinsic defects participating in luminescence process are zinc or oxygen vacancies as well as zinc and oxygen interstitials. The concentration of one or the others depends on stoichiometry, surface states and doping. This explains the fact that the defect luminescence band characteristics are different for single crystal, nanocrystals, thin films and ceramics. Green luminescence with peak position at 2.45 eV can be described with model consisting of the oxygen vacancy (donor) and zinc vacancy (acceptor) as a recombination centers. The yellow (2.2 eV) and red (1.75 eV) luminescence bands are usually associated with impurities. The red luminescence is observed at high temperatures when the green luminescence is quenched [5]; however, the model of red luminescence centers is not known yet.

It is considered that the ZnO is radiation resistant material [7]. However, the intensive thermostimulated luminescence (TSL) is observed after irradiation at $T < 50$ K [6,8]. The TSL after irradiation at $T > 300$ K was observed in several papers: ZnO nanoparticles [9,10], nanorods [11,12] and ceramics [13]. The analysis of published results shows significant difference in peak positions and glow curve intensities in different ZnO samples. TSL peak position depends on ceramic sintering temperature. The irradiation with X-rays results in recharging of defects present before irradiation – not creation of new ones. The origin of TSL is thermal release of charge carriers from defects.

* Corresponding author.
E-mail address: lgrig@latnet.lv (L. Grigorjeva).

http://dx.doi.org/10.1016/j.ceramint.2017.02.016
Received 12 December 2016; Received in revised form 3 February 2017; Accepted 3 February 2017

For dosimetric properties it is important to obtain material with glow peaks at high temperature (excludes the fading effect at room temperature), good TSL reproducibility as well as luminescence spectrum should not coincide or be close to spectrum of heater thermal radiation (far from IR spectral region). The identification of defects responsible for TSL is very important; however, previous publications do not include the strong evidence of the defects involved in TSL as well as any information on luminescence spectral distribution within glow peaks at T > 300 K. ZnO ceramic has only one crystallographic modification and it is easy to prepare as compared with commercial TLD500 dosimeter from α-Al_2O_3:C single crystal.

The main purpose of this research is to study radioluminescence and TSL (including the spectral distribution) in ZnO ceramics fabricated from nanopowders. The use of the same TSL equipment and X-ray irradiation doses allows us to compare the TSL in two different ceramics. The evaluation of the dosimetric characteristics of ZnO ceramics was performed after irradiation with X-rays at room temperature.

2. Experimental procedure

2.1. Synthesis of nanopowders and ceramics

Nanopowders were obtained by two different methods. First method is pulsed electron beam evaporation from metallic Zn target in oxygen atmosphere (32–35 Pa). The method is described in detail in [14,15]. Agglomerated nanopowder of ZnO–Zn in hexagonal phase with a specific surface up to 36 m^2/g was obtained. From this powder the ceramic was sintered (sample 1): nanopowder was pressed in tablets under 800 MPa pressure and then sintered for 60 min at 1200 °C.

The SEM images of initial powder and sample 1 fabricated from it are shown in Fig. 1a and b respectively. The powder is composed from 30 to 50 nm ZnO nanoparticles. The grain sizes in ceramic are 0.8–4.0 μm; density is 3.98 g/cm^3 (or 71% of ZnO crystal density).

Second method used for the synthesis of ZnO nanopowder is the solar physical vapor deposition (SPVD) [16]. The powder was prepared in the Heliotron reactor (PROMES CNRS, France). The SEM image of ZnO nanoparticles is shown in Fig. 2a. The particles have tetrapod form; only hexagonal phase was detected by XRD. From this nanopowder the ceramic sample (sample 2) was sintered in a similar fashion to sample 1: powder weight 0.2 g; tablet prepared under 800 MPa pressure; diameter: 10 mm; sintering temperature: 1100 °C, sintering time: 30 min; sintering atmosphere: air. The SEM image of prepared sample 2 is shown in Fig. 2b.

The grain sizes in sample 2 are 1–4 μm and it contains fewer pores than sample 1.

From the SEM images one can conclude that the physical processes during the sintering of the sample 1 and sample 2 are different; however, this might be due to slight differences in starting nanopowders.

The energy-dispersive X-ray spectroscopy (EDX) measurements show that for e-beam prepared powders the ratio of oxygen concentration to Zn concentration is 18.43/81.57 (wt%), whereas for SPVD powder the ratio is 20.22/79.78 (wt%). Stoichiometric ZnO exhibits the ratio 19.99/80.3 wt%; therefore, the e-beam powder has excess amount of Zn but SPVD powder – excess amount of oxygen. The EDX experiments not showed the presence of impurities, although the presence of residual impurities is not excluded. The luminescence bands due to impurities were not detected.

2.2. Radioluminescence and TSL measurements

The luminescence was measured under X-ray irradiation. X-ray tube (40 kV, 10 mA, W target) with dose rate ~0.3 kGy/min was used for radioluminescence excitation as well as for TSL experiments. The spectra were detected using the Andor Shamrock B-303i spectrometer with a CCD camera Andor DU-401A-BV. The 150 l/mm diffraction grating with the blaze wavelength 800 nm was used. Optical filters were not used on this system during the measurements. The correction for spectral sensitivity was not performed.

The TSL measurements were performed from room temperature up to 700 K with heating rate 2 K/s in vacuum. The thermal irradiation at temperatures above 550 K was taken into consideration and experimentally subtracted from TSL glow curves. Two channels were used for TSL registration. First one (CCD camera, same as for radioluminescence measurements) allows to obtain the spectral distribution of TSL peaks and register data in 3d space (I-T-λ). However, the photosensitivity of this system is low in comparison to photomultiplier tube (PMT); therefore, for the low intensity TSL signal registration Hamamatsu H8259-2 PMT was used. To lower the infrared emission from the heating element, 660 nm shortpass filter was used before photodetector. The both channels were registering TSL signal simultaneously.

SEM and EDX analysis was conducted on SEM electron microscope (Lyra, Tescan).

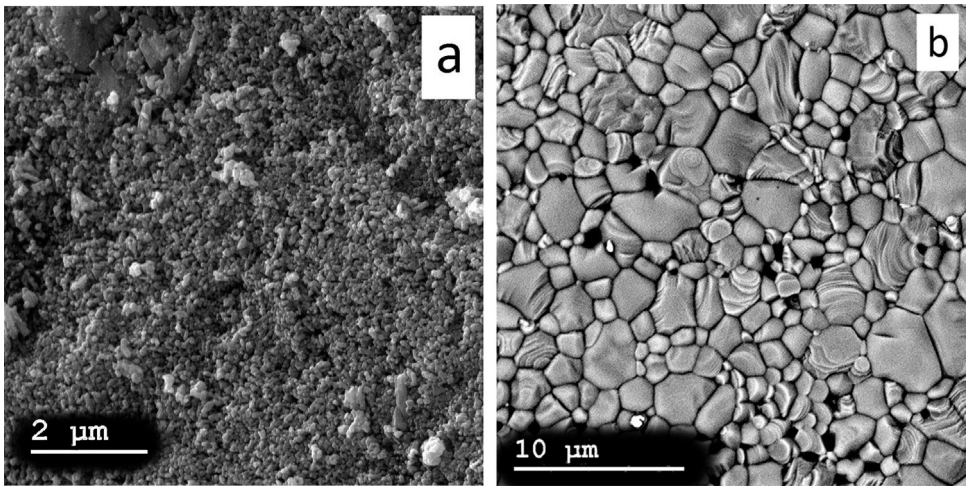

Fig. 1. SEM images of ZnO nanopowder prepared by e-beam evaporation (a) and sample 1 fabricated from this nanopowder (b).

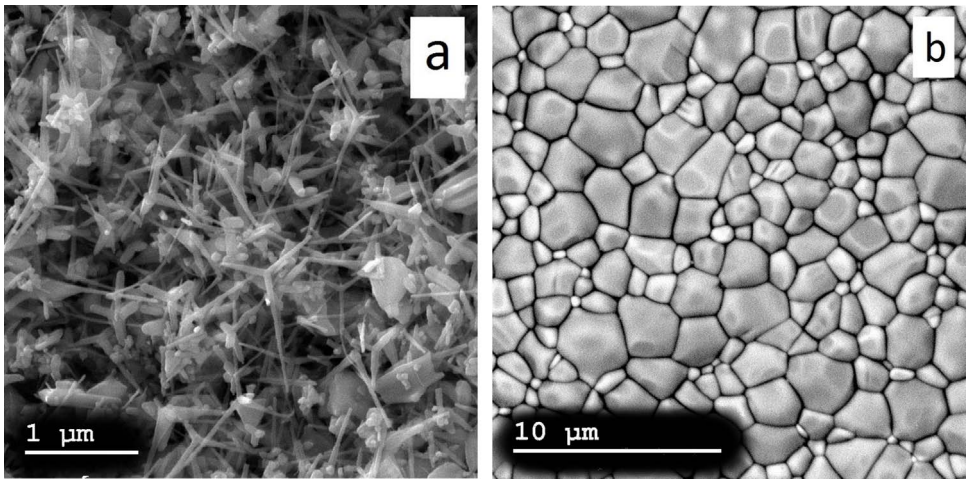

Fig. 2. SEM images of nanopowder prepared by SPVD method (a) and sample 2 fabricated from SPVD nanopowder (b).

3. Results and discussion

3.1. Radioluminescence spectra

3.1.1. Sample 1

Radioluminescence was used for characterization of defect states of studied samples. The radioluminescence spectra at room temperature and at 450 K of sample 1 are shown in Fig. 3. Two groups of luminescence bands – the 375 nm excitonic luminescence (not shown) and 530 nm defect luminescence were observed. The defects luminescence band shape shows that there is contribution from overlapping peaks; therefore, the defect luminescence band was decomposed using two Gaussian peaks at 2.346 eV (528 nm) and 2.09 eV (593 nm). The intensity ratio of these bands is ~3.8 and remained constant for temperatures in 300–500 K range. We estimated the thermal quenching of both components and found that the thermal activation energy is 0.3 eV – same for both bands (Fig. 4). Additional luminescence band in lower energy side of radioluminescence spectra was not detected up to 550 K.

The intensity of X-Ray induced luminescence increases during irradiation and saturates after 60 min. This indicates that the luminescence occurs due to recharging of limited number of defects. In addition, it means that the charge carriers are trapped at defects and TSL is possible.

The normalized spectra measured at the start of the irradiation and after 60 min coincide; therefore, the same defects are responsible for luminescence at initial stage of irradiation and after saturation and the recharging of already existing defects in sample 1 takes place.

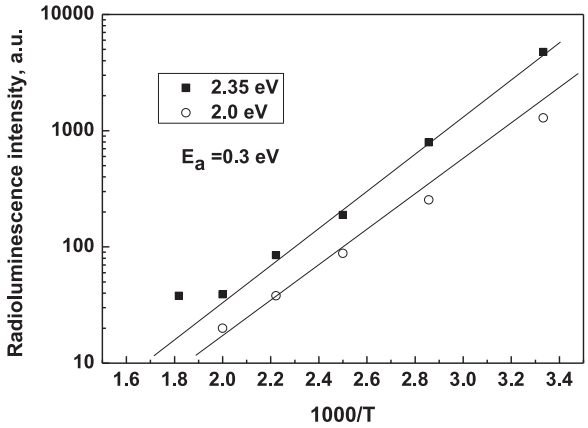

Fig. 4. Arrhenius plot for 2.0 and 2.3 eV bands in sample 1.

3.1.2. Sample 2

The radioluminescence spectra for sample 2 were measured in the same temperature region: 300–550 K. Fig. 5a. shows the radioluminescence spectrum at room temperature. Spectra decomposition gives two Gaussian peaks at ~2.12 eV and ~2.35 eV at 300 K. The peak positions are close to that for sample 1, however, the ratio of amplitudes is ~1.85 at 300 K, considerably different from that for sample 1 (~3.8). This could mean that in sample 2 the contribution of 2.12 eV band in luminescence spectra is higher than in sample 1. Inset in Fig. 5a shows the growth of 2.35 eV peak with irradiation time.

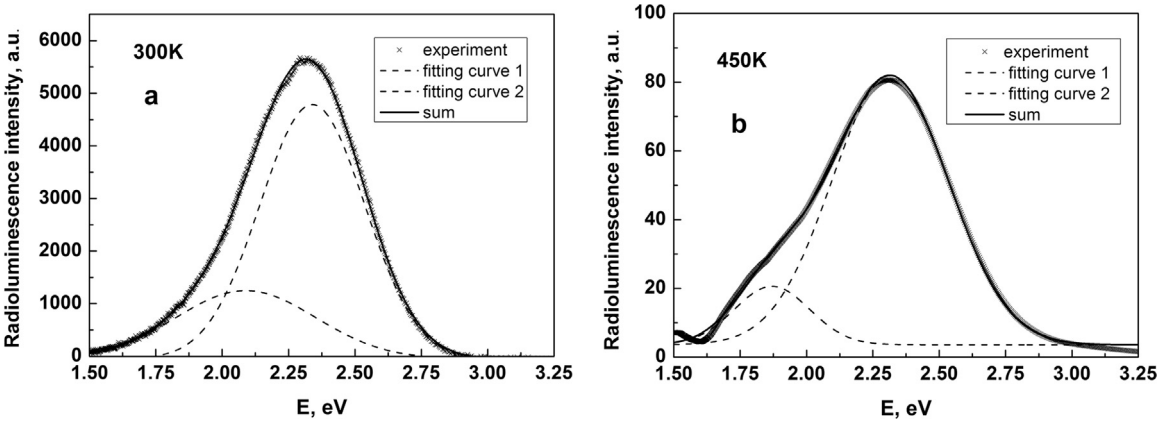

Fig. 3. Radioluminescence spectra at 300 K (a) and at 450 K (b) in sample 1.

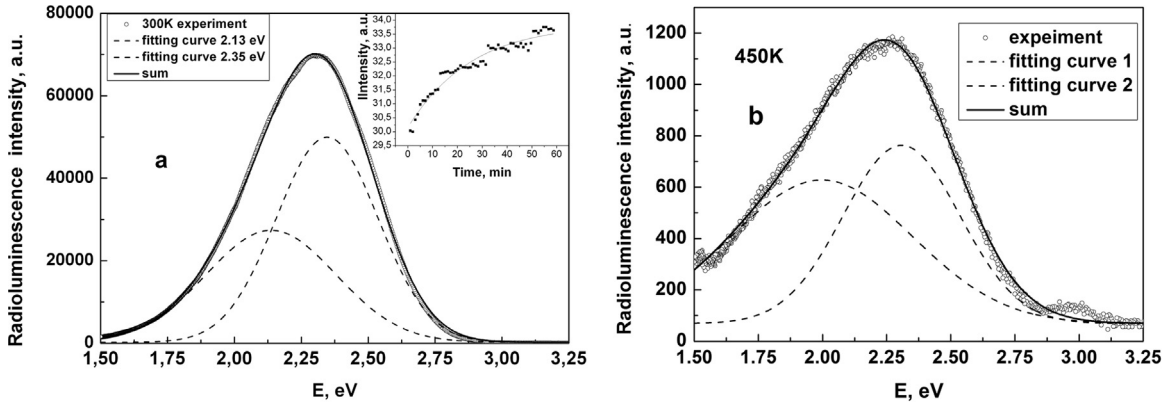

Fig. 5. Radioluminescence spectra at 300 K (a) and at 450 K (b) in sample 2. Inset shows the luminescence intensity dependence on irradiation time.

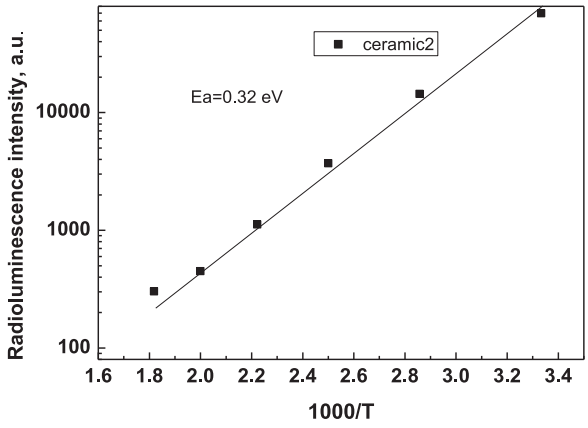

Fig. 6. Arrhenius plot of 2.3 eV band in sample 2.

Intensity increase is non-linear and the saturation occurs after 10 min. Additional short wave bands were not detected in radioluminescence spectra.

The activation energy for green luminescence (2.35 eV) is ~0.32 eV (Fig. 6). For both of the samples the activation energy is approximately the same, which indicates that the luminescence centers are the same in both samples. Slight difference in peak position and activation energy is due to different environment of luminescence centers.

3.2. TSL

3.2.1. Sample 1

After X-ray irradiation at 300 K, several peaks were observed at temperatures 370 K, 420 K and 480 K. TSL glow curves for sample 1 are shown in Fig. 7. The TSL was measured after different irradiation times. Inset shows the peak intensity dependence on acquired radiation dose. The TSL intensity growth is close to linear for irradiation times up to 10 min (TSL signal is proportional to irradiation dose up to ~3 kGy). The intensity of TSL was sufficient for measuring of spectral distribution of luminescence. It is important to note that the TSL spectrum does not coincide with radioluminescence spectra at the same temperatures. Long-wave bands at 2.0 eV and 1.75 eV dominate in TSL spectra whereas the 2.35 eV peak (dominant in radioluminescence) is very weak. Low energy luminescence bands were determined in TSL spectra of ZnO ceramics earlier [8], but for low temperature TSL peaks.

3.2.2. Sample 2

TSL intensity in sample 2 (Fig. 8) is much lower than that in sample 1. Three glow peaks at 370 K, 400 K and 490–520 K were detected. Peak positions are close to those observed for sample 1 suggesting that the traps could be similar; however the trap depth is not the same. The peak intensity ratio is slightly dependent on irradiation dose. Nevertheless, under irradiation up to 30 min (9 kGy) the linear dependence of peak intensity on irradiation dose is observed (insert in Fig. 8). We were unable to record the spectral distribution in TSL maxima for this sample due to the intensity of TSL being too low.

The analysis of results presented in literature [9–13] shows that the position and intensity of TSL peaks vary considerably. Mainly the nanoparticles were under investigation in these studies. Two groups of peaks were reported – 370–480 K and 470–590 K. In some studies the high temperature peak at 620–650 K was observed. TSL and integrated TSL dose dependence was studied for ceramics in [13] and three peaks (450 K, 560 K and 630 K) were detected. After β-particle irradiation, the linear dose dependence in dose range 25–800 Gy with good

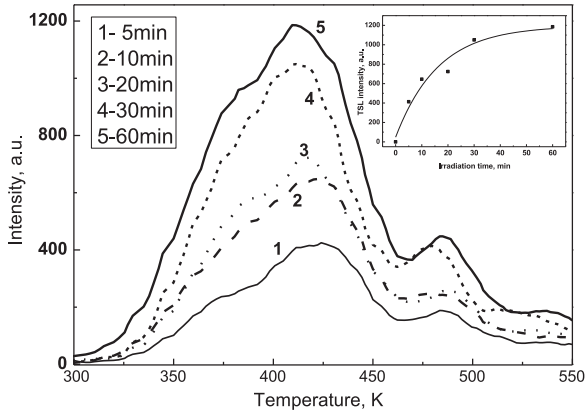

Fig. 7. TSL and TSL intensity dependence on irradiation time (inset) for ceramic 1.

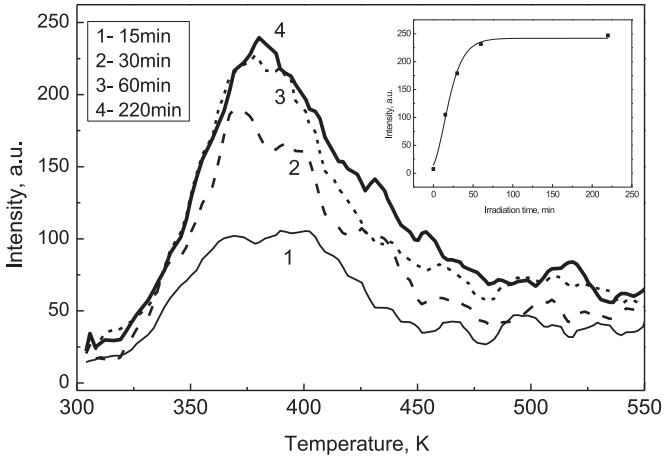

Fig. 8. TSL and TSL intensity dependence on irradiation time (inset) for sample 2.

reproducibility was observed, thus one can conclude that the trap depth in different ZnO materials depends on method of sample preparation. In present study the same experimental equipment was used for TSL measurements in two samples fabricated from different types of nanopowders; however, the peak positions vary only slightly. The peak within 320–450 K range consists of two (~360–375 K and 400–420 K) but the ratio of peak intensities differs in both samples. The peak in temperature region 480–520 K was detected in both samples, but peak position is not the same. It should be noted that not only sintering conditions but also the properties of the initial powder used for ceramic sintering are very important. Both sintering process and raw materials (nanopowders) will determine defect and trap types, their concentration and, consequently, TSL characteristics.

The open question is the nature of the recombination centers in ZnO. It is widely accepted that the green luminescence is due to oxygen vacancies [6 and references therein]. However, the dominant recombination centers in TSL processes are those responsible for 2.0 eV and 1.7 eV luminescence, for example, oxygen interstices (O_i), Li_{Zn} [5].

4. Conclusion

Two ZnO samples were fabricated from ZnO nanopowders synthesized using two different methods. The radioluminescence spectra, TSL glow curves and TSL spectra were studied. The radioluminescence spectra consists of two peaks with peak positions 2.10–2.16 eV (yellow component) and 2.33–2.35 eV (green component). The minor differences in peak positions can be described with different crystal fields of luminescence centers (grain sizes, pores, defects or local stress on grain boundaries). In addition, the ratios of green to yellow luminescence bands intensities are considerably different: ~3.8 for sample 1 and ~1.4 for sample 2. The thermal activation energy is ~0.3 eV for 2.35 eV band in both ceramics. We do not observe the changes in radioluminescence spectra after long irradiation; however, the peak intensity increases and saturation occurs after 60 min. The main TSL peak is in temperature region of 410 K in sample 1 and 380 K in sample 2. Relatively weak TSL peak was observed in 480–520 K temperature region. Consequently, trap depth are different and depend on fabrication method of ceramics and properties of initial powders. The linearity of TSL intensity on irradiation dose was observed in 3–9 kGy dose region; however, the linearity range for dose is different in studied samples.

Acknowledgment

The authors gratefully acknowledge the financial support for this work from research grant ERA.NET RUS Plus Nr.609556 and from the SFERA II project – Transnational Access activities (EU 7th Framework Programme Grant Agreement n° 312643) for supporting ZnO nanopowders preparation.

References

[1] Y. Liu, Y. Li, H. Zeng, ZnO-based transparent conductive thin films: doping, performance, and processing, J. Nanomater. 2013 (1–9) (2013). http://dx.doi.org/10.1155/2013/196521.

[2] J.S. Neal, D.M. DeVito, B.L. Armstrong, M. Hong, B. Kesanli, X. Yang, N.C. Giles, J.Y. Howe, J.O. Ramy, D.W. Wisniewski, M. Wisniewska, Z.A. Munir, L.A. Boatner, Investigation of ZnO-based polycrystalline ceramic scintillators for use as a α-particle detectors, IEEE Trans. Nucl. Sci. 56 (3) (2009) 892–898. http://dx.doi.org/10.1109/TNS.2008.2004702.

[3] J. Wilkinson, K.B. Ucer, R.T. Williams, The oscillator strength of extended exciton states and possibility for very fast scintillators, Nucl. Instr. Methods Phys. Res. A 537 (2005) 66–70. http://dx.doi.org/10.1016/j.nima.2004.07.236.

[4] L. Grigorjeva, D. Millers, K. Smits, A. Zolotarjovs, Gas sensitive luminescence of ZnO coatings obtained by plasma electrolytic oxidation, Sens. Actuators A: Phys. 234 (2015) 290–293. http://dx.doi.org/10.1016/j.sna.2015.09.018.

[5] Ü. Özgür, Ya.I. Alivov, C. Liu, A. Teke, M.A. Reshchikov, S. Doğan, V. Avrutin, S.-J. Cho, H. Morkoç, A comprehensive review of ZnO materials and devices, J. Appl. Phys. 98 (2005). http://dx.doi.org/10.1063/1.1992666.

[6] P.A. Rodnyi, K.A. Chernenko, A. Zolotarjovs, L. Grigorjeva, E.I. Gorokhova, I.D. Venetsev, Effect of point defects on luminescence characteristics of ZnO ceramics, Phys. Solid State 58 (10) (2016) 2055–2061. http://dx.doi.org/10.1134/S1063783416100309.

[7] K. Koike, T. Aoki, R. Fujimoto, S. Sasa, M. Yano, S.-I. Gonda, R. Ishigami, K. Kume, Radiation hardness of single-crystalline zinc oxide films, Phys. Status Solidi (C) 9 (2012) 1577–1579.

[8] O.F. Schirmer, D. Zwingel, The yellow luminescence of ZnO, Solid State Commun. 8 (19) (1970) 1559–1563.

[9] U. Pal, Thermoluminescence properties of ZnO and ZnO:Yb nanophosphors, Appl. Phys. Lett. 89 (2006) 183118.

[10] C. Cruz-Vázquez, H.A. Borbón-Nuñez, R. Bernal, J.A. Gaspar-Armenta, V.M. Castaño, Thermally stimulated luminescence of Mg-doped ZnO nanophosphors, Rad. Eff. Def. Solids 169 (5) (2014). http://dx.doi.org/10.1080/10420150.2014.905943.

[11] P.P. Pal, Photoluminescence and thermoluminescence studies of Tb3+ doped ZnO nanorods, Mater. Sci. Eng. 178 (7) (2013) 400–406. http://dx.doi.org/10.1016/j.mseb.2013.01.006.

[12] P.P. Pal, J. Mnam, Evolution of kinetics parameter in the x-irradiated TSL studies of RE3+-doped (RE=Eu, Tb) ZnO nananorods for dosimetric applications, Rad. Phys. Chem. 88 (2013) 7–13. http://dx.doi.org/10.1016/j.radphyschem.2013.03.023.

[13] H.A. Borbón-Nuñez, C. Cruz-Vázquez, R. Bernal, G. Kitis, C. Furetta, V.M. Castaño, Thermoluminescence properties of sintered ZnO, Opt. Mater. 37 (2014) 398–403. http://dx.doi.org/10.1016/j.optmat.2014.06.034.

[14] V.G. Il'ves, S. Yu, Sokovnin, production of ZnO and Zn–ZnO nanopowders using evaporation by a pulsed electron beam in low pressure gas, Nanotechnol. Russ. 6 (1–2) (2011) 137–143. http://dx.doi.org/10.1134/S199507801101006X.

[15] S. Yu, Sokovnin, V.G. Il'ves, A.I. Medvedev, A.M. Murzakaev, Investigation of properties of ZnO–Zn–Cu nanopowders obtained by pulsed electron evaporation, Inorg. Mater.: Appl. Res. 4 (5) (2013) 410–419. http://dx.doi.org/10.1134/S207511331305016X.

[16] K. Smits, L. Grigorjeva, D. Millers, K. Kundzins, R. Ignatans, J. Grabis, C. Monty, Luminescence properties of zirconia nanocrystals prepared by solar physical vapor deposition, Opt. Mater. 37 (2014) 251–256. http://dx.doi.org/10.1016/j.optmat.2014.06.003.